

Improving the fluorescent properties of polyacrylic acid by adding a mixture of (silver nanoparticles/rhodamine B)

Wesal M Madani¹ · Roshdi Seoudi²

Received: 9 January 2023 / Accepted: 15 March 2023

Published online: 3 April 2023

© The Author(s) 2023 **OPEN**

Abstract

The chemical reduction method was used to prepare silver nanoparticles (AgNPs). The fluorescence spectrum was enhanced by mixing silver nanoparticles with rhodamine B (RhB) and polyacrylic acid (PAA). The surface plasmonic resonance (SPR) of AgNPs was studied using UV–vis spectroscopy to determine the effect of preparation times. TEM measurements confirmed the formation of AgNPs with an average size of 13–19 nm. The Fourier transform infrared bands at 1683 cm^{-1} and 1243 cm^{-1} of PAA have been changed into PAA blended with AgNPs/RhB, due to the interaction between AgNPs and PAA through C=O and C-O functional groups. PAA/(AgNPs/RhB) has high- and low-intensity bands in the UV–visible spectrum. X-ray diffraction analysis was performed on PAA blended with RhB/AgNPs to study the crystallization process. Fluorescence measurements of PAA/(RhB/AgNPs) band emit at 587 nm and 440 nm, with 13–19 nm, respectively. Its emission wavelength is higher than the exciting wavelength, indicating an electronic transition from (SPR) of the nanoparticles and $\pi\text{-}\pi^*$ from RhB to PAA. As a result, adding (AgNPs/RhB) to PAA enhances its fluorescence emission spectrum.

Keywords Silver nanoparticles · Dye-doped polymer · FTIR · Fluorescence

1 Introduction

In recent years, metal nanoparticles have become much more popular due to their colorimetric properties [1]. Nanoparticles have been used in various areas including electronic fields, nanolasers, and optoelectronic devices [2]. Optoelectronic devices, such as optical communication chemical sensors, biosensors, surface-enhanced Raman spectroscopy substrates containing core–shell nanostructures, luminescent nanoparticles, memory devices, and thin film transistors, core–shell nanostructures thin-film solar cells, and fluorescing dyes were manufactured [2–4]. There is a wide variety of methods available for preparing metal nanoparticles, including biological [5], physical

[2], and chemical processes [6]. Several researchers have been interested in silver nanoparticles (AgNPs) because of their unique physical, chemical, optical, and surface properties. Chemical reduction methods are commonly used to prepare AgNPs because they are easily synthesized in solution [7]. Reducing agents, metal precursors, and stabilizing/capping agents are used in chemical reduction [7]. Several studies have demonstrated that AgNPs can form hexagonal, spherical, fibers, cubic, prisms, shells [8], and nanowires [9]. In metal nanoparticles, surface plasmon resonance is characterized [6]. In metal nanoparticles, light incident on their surfaces generates free conduction electrons via surface plasmon resonance (SPR). This phenomenon can only be realized by metal nanoparticles with

✉ Wesal M Madani, wesal.md@gmail.com; Roshdi Seoudi, rsmawed@yahoo.com | ¹Department of Physics, College of Applied Science, Umm Al-Qura University (UQU), Makkah, Saudi Arabia. ²Spectroscopy Department, Physics Research Institute, NRC, Dokki 12622, Cairo, Egypt.



a dimension smaller than the wavelength of the incident light [10, 11]. A metal nanoparticle's optical properties are dependent on its shape and size [12, 13]. By combining silver nanoparticles with organic or inorganic chromophores, light properties can be enhanced compared to other particles of the same size [1]. Using polymers as stabilizing agents or coating agents can prevent nanoparticles from aggregating by changing their surface atomic structure [14, 15]. The two main types of polymers are semicrystalline and amorphous [16]. Researchers have extensively studied and applied metal nanoparticles to polymers to provide new properties [17]. Scientists are intrigued by the study of metal nanoparticles and dyes doped in polymers because of their applications in photodetectors, light-emitting diodes, solar cells, solid-state lasers, and optical sensitivity [18, 19]. Rhodamine B (RhB) is an organic dye, dissolved in water and ethanol due to electron donor and electron acceptor groups [20, 21]. Additionally, it emits fluorescence in the ultraviolet and visible ranges of the electromagnetic spectrum [22]. A fluorescent molecule produces light with a wavelength longer than that of excited light [10]. This work aims to improve the emission spectra of RhB/AgNPs doped polyacrylic acid by adding different sizes and shapes of silver nanoparticles. A variety of silver nanoparticles (shapes and sizes) can be prepared using chemical reduction methods, including spheres and nanorods with different aspect ratios. Based on the results, it can determine which sample provides the highest fluorescence intensity for use as an active laser.

2 Materials and methods

2.1 Materials

The purity rating of silver nitrate (AgNO_3) is > 99.0%, the purity rating for sodium borohydride (NaBH_4) is 99.99%, the purity of trisodium citrate ($\text{C}_6\text{H}_5\text{Na}_3\text{O}_7 \cdot 2\text{H}_2\text{O}$) is 99.8%, and the molecular weight of polyacrylic acid is 450,000 g/mol [$\text{C}_3\text{H}_4\text{O}_2$]. All these materials were purchased from Sigma-Aldrich (USA). Rhodamine B ($\text{C}_{28}\text{H}_{31}\text{ClN}_2\text{O}_3$) was purchased from ACROS (USA) for approximately 95% of the dye. A pale green to very dark green color is typical of the dye, while a bright pink color is characteristic of the soluble form.

2.2 Preparation of AgNPs

For the preparation of silver nanoparticles, 0.10185 g of AgNO_3 was dissolved in 600 ml of deionized water (D.W) at a concentration of 1 mM and heated at 80 °C with magnetic stirring. Trisodium citrate at a concentration of (3.4×10^{-4} M) was added to the solution as a capping agent, followed by

5 μL of NaBH_4 at a concentration of 1 M as a reducing agent. The mixture turned yellow as Ag nanoparticles grew. The sample was removed from the hot plate as soon as the color changed and allowed to cool at room temperature. To prepare samples (S1—S6), 100 ml was taken from the mixture at different times ($t=0.5, 1.0, 3.0, 7.0, 11, 25$ min).

2.3 Fabrication of PAA doped by (RhB/AgNPs) thin films

For the preparation of 4% concentration of PAA (450,000 g/mol), eight grams were added to 200 ml of distilled water. A 5 ml PAA solution was heated until completely dissolved, then poured onto a 9 cm petri dish to form a thin film. 0.74901 g of RhB was dissolved in 100 ml of distilled water under magnetic stirring at room temperature to obtain a solution of (1×10^{-3} M) of RhB. Dye-doped PAA films were prepared by mixing various amounts of RhB (5 M) with AgNPs in 5 ml of pure PAA. A thin film of the mixture was formed at room temperature by pouring it into a 9 cm petri dish.

2.4 Samples characterization

The absorbance spectrum of AgNPs colloidal was measured using a UV–VIS–NIR spectrophotometer (Thermo-scientific Evolution 220) with a resolution of 2 nm. Fourier Transform Infrared Spectrometer (FTIR) Jasco Model 300E was used to measure vibrational spectra. A transmission electron microscope (TEM) was used to analyze morphology samples and calculate particle sizes. On carbon-coated copper grids with 200 mesh, the sample solution was placed and allowed to air dry. On the samples, TEM was performed using a JEOL JEM-1100 microscope (JEOL Ltd., Tokyo, Japan) equipped with a 100-kV tungsten thermionic gun. CCD camera was used to acquire TEM images. The X-ray diffraction pattern was measured by CuK α radiation at 40 kV and 40 mA, and λ of 1.5406 Å. Scanning speeds of 0.02°/s were achieved from 30° to 90°. The nanoparticle crystal size was calculated using Scherrer's formula. Morphological characterization was performed using a scanning electron microscope (SEM) (JSM-6380 LA). Fluorescence spectra were measured using a Jasco FP-777 spectrofluorometer. In this case, the light source is a 150-W Xenon arc lamp.

3 Results and discussions

3.1 An investigation of the Uv–Vis properties of silver nanoparticles

A UV–visible spectrum for Ag nanoparticles is shown in Fig. 1. All samples (S1–S6) exhibited an absorption peak at

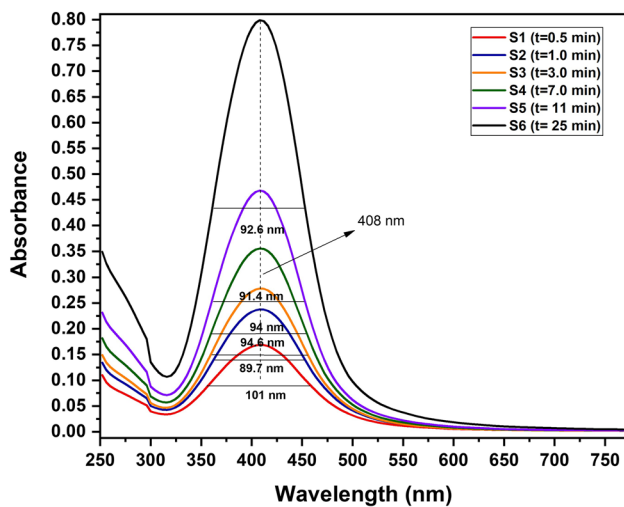


Fig. 1 The absorbance spectra of silver nanoparticles were synthesized at (80 °C) and at different times

408 ± 3 nm. This phenomenon is called surface plasmon resonance (SPR) and indicates the formation of AgNPs. Based on Krasovskii et al. and Kudelski et al. [23, 24], SPR mechanism relies on the resonance between the collective oscillations of electrons in AgNPs and external electromagnetic waves. There is no change in Plasmon band positioning with heating time. This may be due to the combination of trisodium citrate and AgNPs, which stabilizes AgNPs through electronegativity. The adsorption intensity of the bands increased with increasing heating time as AgNPs in the solution increased. The half-bandwidth decreased over time, dropping from 101 nm to 92.6 nm between 0.5 and 15 min. The decrease with time indicates a decrease in aggregation between the nanoparticles in the solution and an increase in interparticle spacing.

3.1.1 The UV–visible spectrum of PAA doped with RhB/AgNPs

Figure 2a shows the absorption spectra of PAA doped with RhB/AgNPs (13 nm). A polyacrylic acid (PAA) film is transparent and does not exhibit an absorption band at visible wavelengths, whereas RhB exhibits an absorption band at 552 nm, as shown inset Fig. 2a. As a result of the addition of both AgNPs and RhB, a strong band at 560 nm and a low-intensity band at 408 nm. The first band is due to RhB, while the second band owing to AgNPs. This may be caused by surface plasmon bands of silver nanoparticles with the RhB interfering with each other to see the band at (552 nm). RhB molecules interact with AgNPs, causing an electrostatic distribution around RhB to change, PAA to shrink, and the distances between AgNPs to decrease. In response to the increased aggregation of RhB molecules,

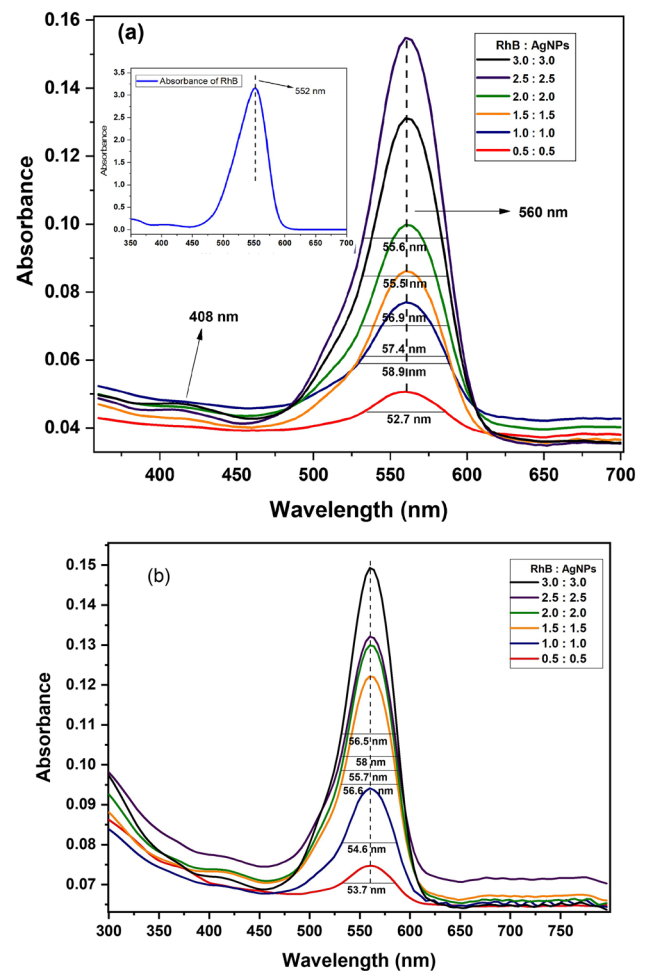


Fig. 2 a, b Ultraviolet–visible spectra of PAA films doped with RhB/AgNPs (13 nm) and RhB/AgNPs (19 nm) at different mole ratios

red shifts were observed [25]. Additionally, the PAA-doped film has a higher color intensity, so the intensity of the absorbance band at 560 nm increases with increasing AgNPs and RhB molar concentrations. In contrast, the half-bandwidth decreased because PAA stabilized AgNPs with RhB. Because of the fewer AgNPs, the absorption band PAA-doped by RhB and AgNPs (19 nm) in Fig. 2b began to weaken.

3.1.2 Analysis of PAA and PAA containing RhB/AgNPs by FTIR

FTIR spectra of PAA and PAA doped with RhB/AgNPs (13 nm and 19 nm) are shown in Fig. 3(a, b). PAA showed two absorbance bands at 3424–3349 cm⁻¹ corresponding to O–H and –CO(OH) stretching vibrations. These bands changed to 3438 cm⁻¹ and 3338 cm⁻¹ in the spectra of PAA doped by RhB/AgNPs. As a result of the interaction between the –CO (OH) groups and AgNPs. PAA doped with

RhB/AgNPs recorded an unchanged band at 2944 cm^{-1} , which was interpreted as the CH_2 stretching vibration. In addition, the overtone and combination of C-O and C-H groups at 2645 cm^{-1} remained unchanged. It is possible to observe two bands at 1712 cm^{-1} and 1689 cm^{-1} , which corresponded to C=O stretching vibration in PAA. As the second band disappears in the PAA demonstrates the interaction between AgNPs and the C=O group. By embedding AgNPs/RhB into PAA, the bending vibration band at 1436 cm^{-1} which is assigned to C-O-H has been widened. The absorbance band appeared 1243 cm^{-1} which is characteristic of the OH bending vibration in PVA, and appeared in PAA-doped systems, also. The band observed at 1197 cm^{-1} in PAA, associated with C-O-H groups became 1199 cm^{-1} in the doped PAA. The band at 802 cm^{-1} attributed to C-COOH stretching vibrations was unchanged in the doped PAA. Figure 3 (a, b) shows

no appreciable difference between PAA doped with RhB and AgNPs at two different sizes (13 and 19 nm) except for differences in intensity. AgNPs with two sizes were chemically or electrostatically attached to PAA through the C=O group.

3.2 The TEM image of silver nanoparticles

Figure 4 (a) shows AgNPs prepared at 80°C for one minute. AgNPs are usually spherical or prism-shaped and appear as dark spots. According to the relationship between repeated particles of the same size (frequency%) and those of different sizes in Fig. 4 (b), the average particle size is 13 nm. In TEM images of AgNPs prepared at 80°C for 3 min, hexagonal, cylindrical, and spherical shapes can be seen in the prepared sample. The average particle size of 19 nm is shown in Fig. 4 (d).

3.3 X-Ray diffraction of PAA doped with RhB/AgNPs

Figure 5(a, b) depicted the x-ray diffraction pattern intensity of PAA doped with RhB/AgNPs (13 nm) and RhB/AgNPs (19 nm). Diffraction pattern peaks at 37.41° , 43.67° , 63.94° , 77° , and 81.23° have varying intensities and correspond to the planes (111), (200), (220), (311), and (222), respectively.

The results were similar to those obtained from (International Center for Diffraction Data, JCDs 4–0783) [26]. It was found that the diffraction pattern and the Bragg reflection of the silver nanoparticle were similar. The results indicate that AgNPs possess a face-centered cubic (fcc) structure, which is consistent with the findings of Mollack et al. [27]. The crystal sizes at each peak were estimated using Scherrer's formula $D = \frac{0.9\lambda}{\beta \cos \theta}$, [28]. The formula consists of, D being the crystal size, θ is the Bragg angle, β is the half-bandwidth broadening of the X-ray peak, and λ is the X-ray wavelength (1.540562 \AA). The (Intensity peak/maximum intensity) was multiplied by the crystal sizes of each peak. The crystal sizes were estimated at 48 nm, 30 nm, 38 nm, 32 nm, and 57 nm for (37.41° , 43.67° , 63.94° , 77° , and 81.23°) peaks as well as 48 nm, 42 nm, 43 nm, 31 nm, and 28 nm for the peak position at (37.38° , 43.63° , 63.95° , 77.01° , and 81.21°) in PAA doped by RhB/AgNPs (13 nm) and RhB/AgNPs (19 nm), respectively. Therefore, the average peak size calculated for the two samples was 41 nm and 42 nm, respectively. There is a difference between the average estimate of crystal size and the value of each peak because each peak has a different intensity. X-ray peak half-bandwidth broadening was inversely related to AgNPs crystal size. As a result of attributable particle sizes, PAA doped with AgNPs (13 nm) has a lower peak intensity than AgNPs (19 nm). Particle sizes calculated from TEM are smaller than those calculated from

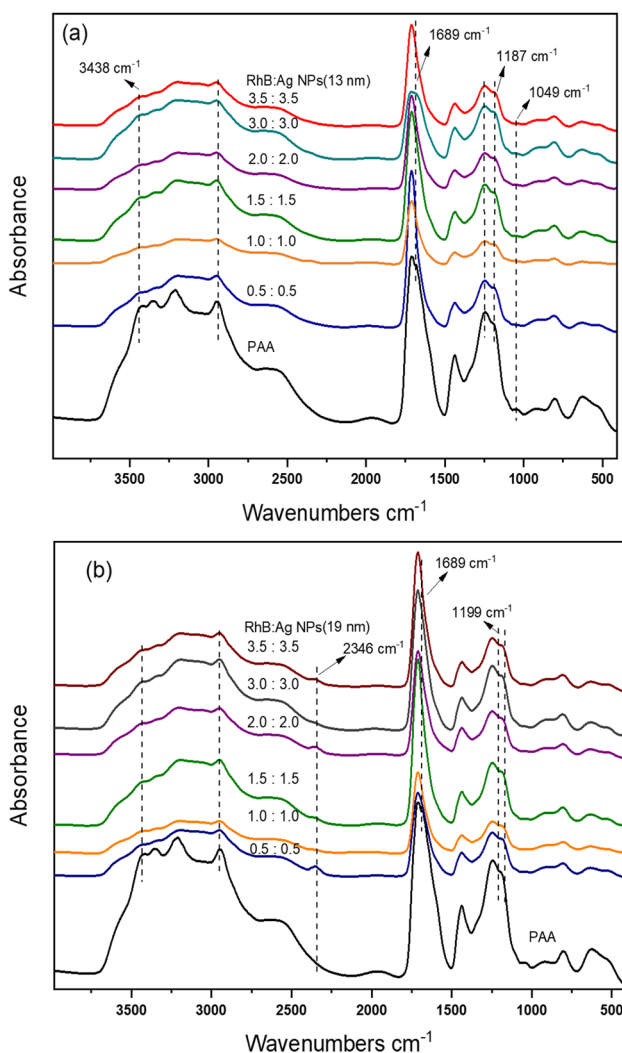


Fig. 3 a, b Infrared spectra of PAA films doped with RhB/AgNPs (13) and RhB/AgNPs (19 nm) with varying molar ratios

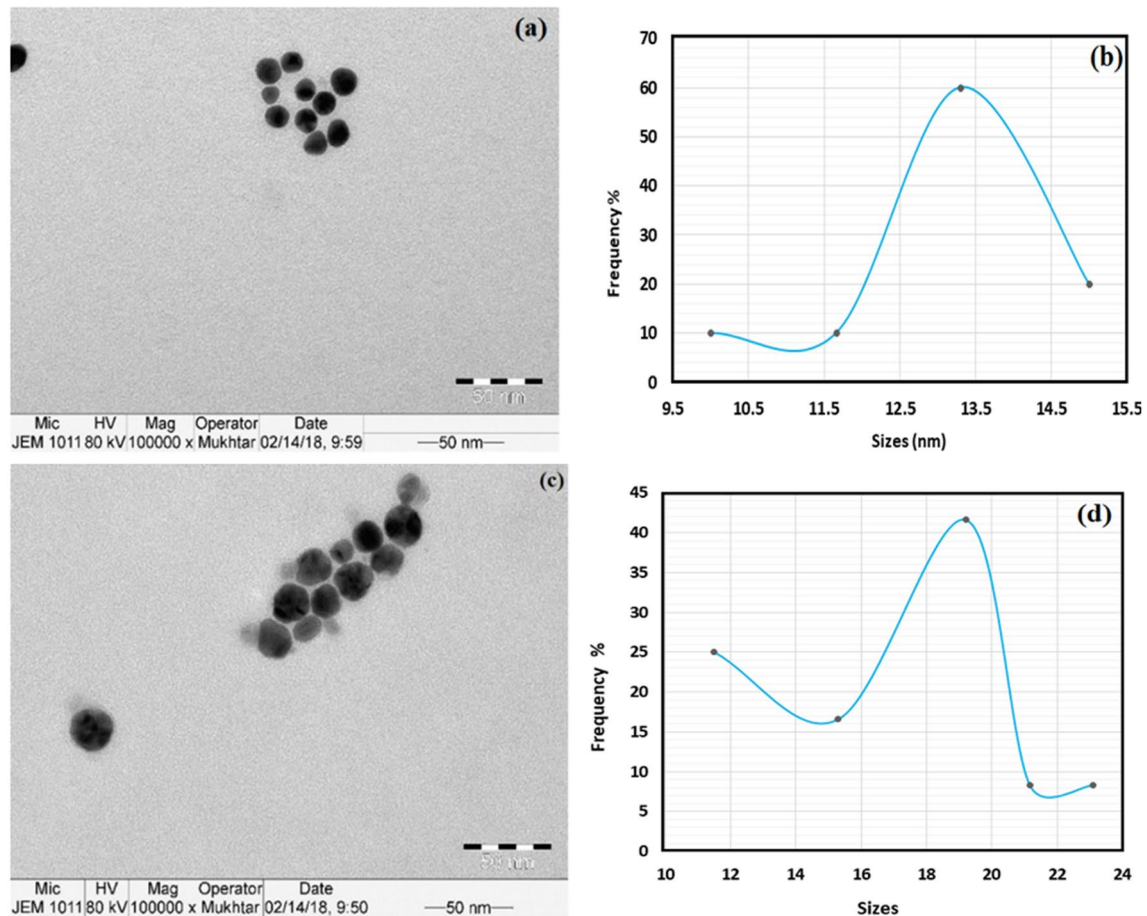


Fig. 4 a–d Transmission electron microscopy images of (a) silver nanoparticles prepared at 80 °C for 1 min, (b) frequency % as a function of particle sizes, (c) silver nanoparticles prepared at 80 °C and time 3 min, (d) frequency % as a function based on particle size

X-rays. The reason for this may be that several AgNPs were collected during the preparation of the PAA doped with AgNPs/RhB. It also observed that Bragg peaks appeared near fundamental peaks. According to Karthik et al. [29], these peaks may be caused by capping agents around AgNPs, as noted by Karthik et al. [29], or by impurities on RhB crystals and an amorphous organic phase seen in the results as reported by Jain and Mehata [30].

3.4 SEM analysis of PAA doped with RhB/AgNPs

A scanning electron microscope (SEM) image of PAA film doped with RhB/AgNPs (13 nm) and RhB/AgNPs (19 nm) is shown in Fig. 6 (a, b). In Fig. 6 (a), AgNPs of sizes (13 nm) appeared as white spots with various (spherical, popcorn, and cylinder). Additionally, particles were distributed randomly throughout the whole image. As shown in Fig. 6 (b), AgNPs (19 nm) aggregate into large white particles when added to RhB and embedded in PAA, they aggregate into large white particles with various shapes, as shown in Fig. 6 (b). Based on the SEM images, it is apparent that the

particles in the TEM images (13 nm and 19 nm), are smaller than those in the post-doped images when measured against their PAA-doped counterparts. It is possible that some agglomeration occurred during the preparation of RhB/AgNP-doped PAA. It is possible that some agglomeration occurred during the preparation of RhB/AgNP-doped PAA.

3.5 Fluorescence of PAA doped by RhB/AgNPs

Figure 7(a, b) shows the fluorescence spectra of a transparent (PAA) doped with two equivalent amounts of RhB/AgNPs (13 nm) and RhB/AgNPs (19 nm) between (380 nm–680 nm). To release fluorescent light, samples were excited at 408 nm (the surface plasmon band of AgNPs discussed in UV–Vis results). In Fig. 7 (a), the fluorescence bands of PAA doped by RhB/AgNPs at 440 nm, 443 nm, 439 nm, 439 nm, and 440 nm represent the emission from silver nanoparticles (13 nm) mixed with RhB, where (AgNPs: RhB) is (1.0: 1.0), (1.5: 1.5), (2.0: 2.0), (2.5: 2.5), and (3.0: 3.0). The bands at 588 nm, 591.5 nm, 585.5 nm,

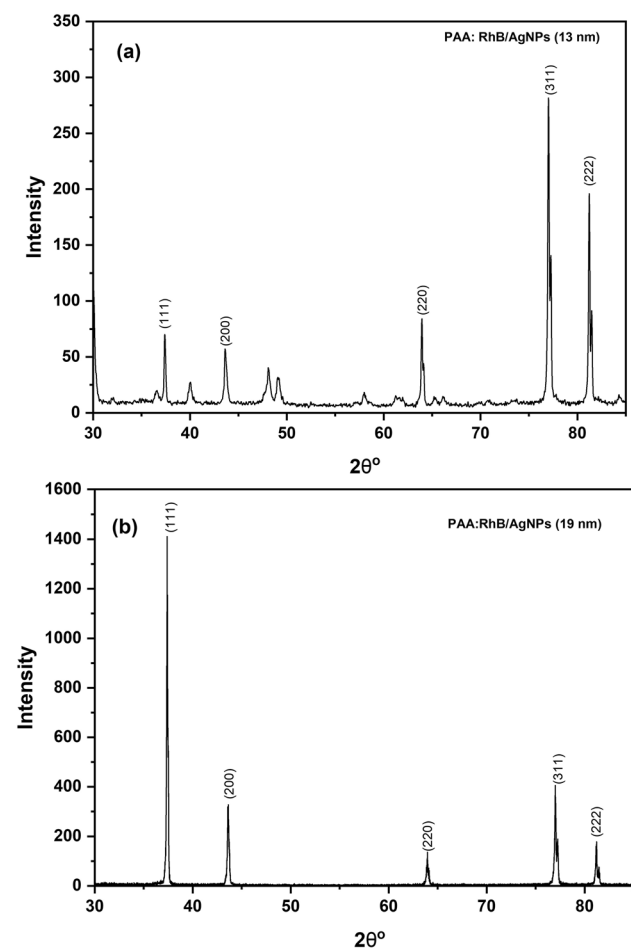


Fig. 5 The X-ray diffraction pattern of PAA film doped with two equivalent amounts of RhB/AgNPs (a) AgNPs (13 nm) and (b) AgNPs (19 nm)

585.5 nm, and 585 nm of RhB/AgNPs (13 nm) with the ratios above refer to emissions from RhB. The intensity of emissions spectra increased in response to increases in the concentrations of RhB/AgNPs (13 nm). The emission of fluorescence at longer wavelengths was lower than at shorter wavelengths. Because of the surface plasmon band of AgNPs, the exciting wavelength of 408 nm weakens the effect on RhB fluorescence. In spite of this, the fluorescence of AgNPs is substantially affected. Regardless of the emission bands, the intensity of emissions can change with strange behavior the molar ratio of AgNPs/RhB (color groups) was not directly affected. Observed behaviors are similar to those observed in previous studies by Jana et al. [10] and B. Paul et al. [31]. As a result of (2:2 ml) molar ratios of AgNPs/ RhB, maximum intensities were observed at 440–590 nm. The ratios indicate that AgNPs/RhB exhibit an increased electric transition between color-bearing groups. Silver nanoparticles saturated the PAA film at that point (3.0 mL: 3.0 mL), decreasing the fluorescence

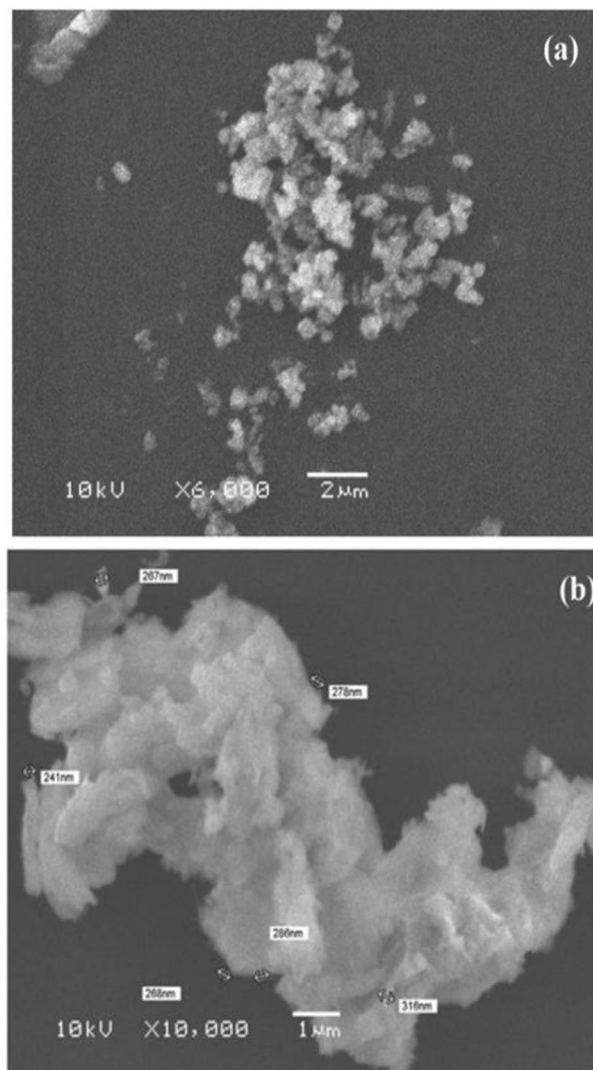


Fig. 6 a, b Scanning electron microscope (SEM) images of PAA film doped with two equivalent amounts of RhB/AgNPs (a) AgNPs (13 nm) and (b) AgNPs (19 nm)

intensity [32]. Based on our observations, RhB has assembled on AgNPs surfaces. As a result, the fluorescence intensity of AgNPs decreases. An important characteristic of PAA-doped films is the Stokes shift formula, which describes the difference in dipole moments between the ground state (S_0) and the first excited state (S_1).

$$\nabla\lambda = \lambda_f - \lambda_a \quad (1)$$

where λ_f and λ_a represent the wavelengths of fluorescence and maximum absorbance, respectively. Table 1 shows the Stokes shift values.

By changing the molar ratio of AgNPs/RhB in Table 1, the Stokes shift was changed, indicating that AgNPs and RhB molecules show different fluorescence self-absorption.

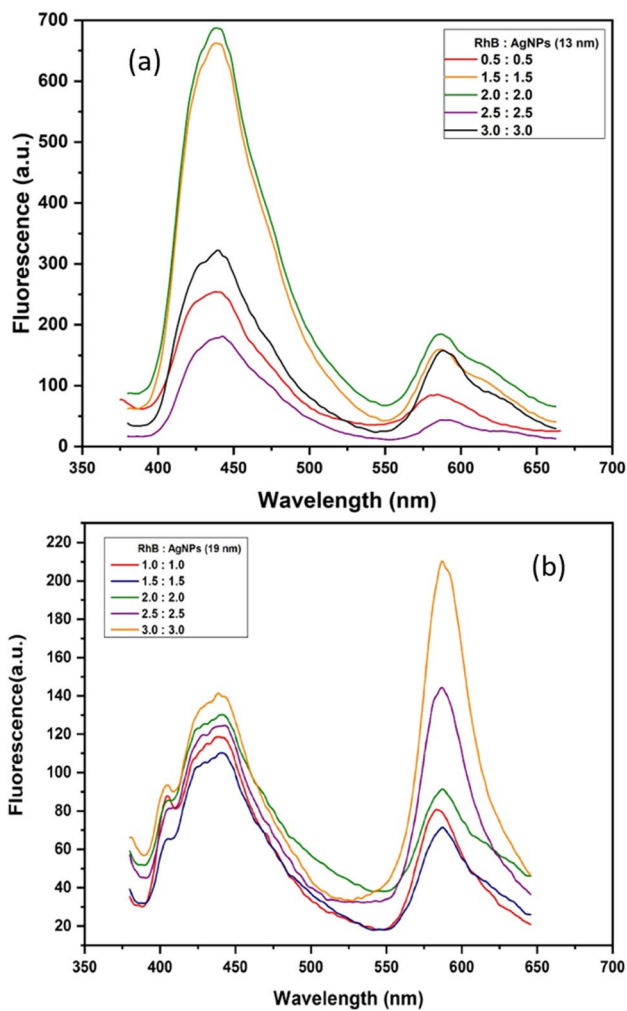


Fig. 7 **a, b** Fluorescence spectra of PAA films doped with RhB and AgNPs (13 and 19 nm) at different molar ratios

The fluorescence emission of AgNPs at 438 nm in PAA-doped by RhB/AgNPs (19 nm) is shown in Fig. 7b. In PAA doped with RhB/AgNPs (19 nm), the RhB emission bands appeared at 587 nm, 586.5 nm, 587 nm, 587 nm, and 583 nm, respectively. These values were obtained with molar ratios of (1.0: 1.0), (1.5: 1.5), (2.0: 2.0), (2.5: 2.5), and (3.0: 3.0). There is no relationship between fluorescence intensity and the molar ratio of AgNPs/RhB doped in PAA [31]. There was no apparent shift in the emission bands. Fluorescence spectra of AgNPs/RhB have decreased in intensity due to more nanoparticle aggregation, which has caused an accumulation of RhB, thereby decreasing fluorescence intensity. The maximum absorbance intensity was found at (3.0: 3.0) molar ratio of AgNPs/RhB. The electric transition between AgNPs and RhB molecules contributes to the color-bearing groups in RhB molecules [32]. Table 1 shows that the Stokes shift increases as AgNPs/RhB molar ratio increases, resulting in a steady rate of fluorescence spectrum absorption by AgNPs (19 nm) and RhB molecules. Because AgNPs and RhB are close to each other, the difference in fluorescence between PAA doped (RhB/AgNPs (13 nm) and PAA doped (RhB/AgNPs (19 nm) can be explained by the strong interaction between AgNPs/RhB.

4 Conclusion

Silver nanoparticles (AgNPs) were prepared in a variety of forms and sizes. UV–visible spectra of PAA doped by RhB/AgNPs showed two bands at 560 nm and 408 nm. According to FTIR spectra, the bands at 1683 cm^{-1} and 1243 cm^{-1} attributed to both C=O and C-O of PAA have been shifted due to electrostatic interactions between AgNPs and PAA through C=O and C-O functional groups. The formation of

Table 1 Photophysical properties of PAA films containing RhB and AgNPs at equivalent molar ratios (13 and 19 nm)

Polymer	Molar ratio RhB: AgNPs (13 nm)	Absorption wavelength (λ_a)	Fluorescence wavelength (λ_f)	$\nabla\lambda = \lambda_f - \lambda_a$
PAA	0.5: 0.5	408 nm	440 nm	32 nm
	1.5: 1.5	408 nm	439 nm	31 nm
	2.0: 2.0	408 nm	439 nm	31 nm
	2.5: 2.5	408 nm	443 nm	35 nm
	3.0: 3.0	408 nm	440 nm	32 nm
Polymer	Molar ratio RhB: AgNPs (19 nm)	Absorption wavelength (λ_a)	Fluorescence wavelength (λ_f)	$\nabla\lambda = \lambda_f - \lambda_a$
PAA	1.0:1.0	408 nm	7	30 nm
	1.5: 1.5	408 nm	438 nm	30 nm
	2.0: 2.0	408 nm	438 nm	30 nm
	2.5: 2.5	408 nm	438 nm	30 nm
	3.0: 3.0	408 nm	438 nm	30 nm

spherical AgNPs with two different sizes at 13–19 nm was confirmed by TEM analysis. X-ray diffraction study of RhB/AgNPs doped PAA revealed a crystalline structure, and crystal sizes were determined using Scherrer equations at 41–42 nm. Particle sizes calculated from SEM images and X-ray diffraction are higher than those calculated from TEM images due to nanoparticle aggregation during the incorporation of AgNPs into PAA. Fluorescence spectra of PAA doped with RhB/AgNPs (13–19 nm) at various molar ratios revealed that RhB and AgNPs emit emission bands at 587 nm and 440 nm, respectively. Higher bands are explained by electronic transitions from surface plasmon resonances of AgNPs and π - π^* of RhB to PAA. Therefore, AgNPs/RhB doped in PAA film enhanced the fluorescence spectra, meaning these samples could be used for laser dye enhancement.

Acknowledgements The authors thanks all member of the physics department of Umm Al Qura university for helping during the preparation of this manuscript.

Authors' contributions The manuscript title “Improving the Fluorescent Properties of Polyacrylic Acid by Adding A Mixture of (Silver Nanoparticles/Rhodamine B)”. Authors: WM (corresponding author): performed the experiments; Analyzed and interpreted the data; wrote the paper. RS: conceived and designed the experiments; Analyzed and interpreted the data; Wrote the paper; Reviewed and Editing. All authors have read and agreed to the published version of the manuscript.

Funding The authors declare that no funding in the manuscript file.

Data availability The authors declare that they have included all data availability statement in the main manuscript file.

Declarations

Conflict of interest The authors declare that they have no known competing financial interests or personal relationships that could have appeared to influence the work reported in this paper.

Open Access This article is licensed under a Creative Commons Attribution 4.0 International License, which permits use, sharing, adaptation, distribution and reproduction in any medium or format, as long as you give appropriate credit to the original author(s) and the source, provide a link to the Creative Commons licence, and indicate if changes were made. The images or other third party material in this article are included in the article's Creative Commons licence, unless indicated otherwise in a credit line to the material. If material is not included in the article's Creative Commons licence and your intended use is not permitted by statutory regulation or exceeds the permitted use, you will need to obtain permission directly from the copyright holder. To view a copy of this licence, visit <http://creativecommons.org/licenses/by/4.0/>.

References

- Oliveira E, Núñez C, Santos H, Fernández-Lodeiro J, Fernández-Lodeiro A, Capelo J, Lodeiro C (2015) Revisiting the use of gold and silver functionalised nanoparticles as colorimetric and fluorometric chemosensors for metal ions. *Sens Actuators, B Chem* 212:297–328. <https://doi.org/10.1016/j.snb.2015.02.026>
- Prakash A, Pathrose B, Nampoori V, Radhakrishnan P, Mujeeb A (2019) Thermal diffusivity of neutral red dye using dual beam thermal lens technique: a comparison on the effects using nano pulsed laser ablated silver and gold nanoparticles. *Physica E* 107:203–208. <https://doi.org/10.1016/j.physe.2018.10.001>
- Wang H, Qiao X, Chen J, Ding S (2005) preparation of silver nanoparticles by chemical reduction method. *Colloids Surf, A* 256:111–115. <https://doi.org/10.1016/j.colsurfa.2004.12.058>
- Ning S, Wu Z, Dong H, Ma L, Jiao B, Ding L, Ding L, Zhang F (2016) The enhanced random lasing from dye-doped polymer films with different-sized silver nanoparticles. *Org Electron* 30:165–170. <https://doi.org/10.1016/j.orgel.2015.12.021>
- Gudikandula K, Maringanti S (2016) Synthesis of silver nanoparticles by chemical and biological methods and their antimicrobial properties. *J Exp Nanosci* 11:714–721. <https://doi.org/10.1080/17458080.2016.1139196>
- Han J, Gurunathan S, Jeong J, Choi Y, Kwon D, Park J, Kim J (2014) Oxidative stress mediated cytotoxicity of biologically synthesized silver nanoparticles in human lung epithelial adenocarcinoma cell line. *Nanoscale Res Lett* 9:459. <https://doi.org/10.1186/1556-276x-9-459>
- Gurunathan S, Jeong J, Han J, Zhang X, Park J, Kim J (2015) Multidimensional effects of biologically synthesized silver nanoparticles in helicobacter pylori, helicobacter felis, and human lung (I132) and lung carcinoma A549 cells. *Nanoscale Res Lett* 10:1–17. <https://doi.org/10.1186/s11671-015-0747-0>
- Fahmy A, Eisa W, Yosef M, Hassan A (2016) Ultra-thin films of poly(acrylic acid)/silver nanocomposite coatings for antimicrobial applications. *J Spectrosc* 2016:1–11. <https://doi.org/10.1155/2016/7489536>
- Liz-Marzán M (2004) Nanometals: formation and color. *Mater Today* 7:26–31. [https://doi.org/10.1016/S1369-7021\(04\)00080-X](https://doi.org/10.1016/S1369-7021(04)00080-X)
- Jana J, Ganguly M, Pal T (2016) Enlightening surface plasmon resonance effect of metal nanoparticles for practical spectroscopic application. *RSC Adv* 6:86174–86211. <https://doi.org/10.1039/c6ra14173k>
- Madami W, Seoudi R (2020) Molecular and fluorescence spectroscopic studies of polyacrylic acid blended with rhodamine B mixed gold nanoparticles. *J Taibah Univ Sci* 14:790–799. <https://doi.org/10.1080/16583655.2020.1776460>
- Nedyalkov N, Dikovska A, Koleva M, Stankova N, Nikov R, Borisova E, Genova T, Aleksandrov L, Iordanova R, Terakawa M (2020) Luminescence properties of laser-induced silver clusters in borosilicate glass. *Opt Mater*. <https://doi.org/10.1016/j.optmat.2019.109618>
- Wang W, Ramezani M, Väkeväinen A, Törmä P, Rivas J, Odom T (2018) The rich photonic world of plasmonic nanoparticle arrays. *Mater Today* 21:303–314. <https://doi.org/10.1016/j.mattod.2017.09.002>
- Bhushan B, Luo D, Schrickler S, Sigmund W, Zauscher S (2014) Handbook of nanomaterials properties. Springer, Berlin Heidelberg, Berlin
- Tommaliéh M, Awwad N, Ibrahim H, Menazea A (2021) Characterization and electrical enhancement of pvp/pva matrix doped by gold nanoparticles prepared by laser ablation. *Radiat Phys Chem*. <https://doi.org/10.1016/j.radphyschem.2020.109195>

16. Ragab H, Rajeh A (2020) Structural, thermal, optical and conductive properties of pam/pva polymer composite doped with ag nanoparticles for electrochemical application. *J Mater Sci: Mater Electron* 31:16780–16792. <https://doi.org/10.1007/s10854-020-04233-6>
17. Morsi M, El-Khodary S, Rajeh A (2018) enhancement of the optical, thermal and electrical properties of peo/pam:li polymer electrolyte films doped with ag nanoparticles. *Physica B* 539:88–96. <https://doi.org/10.1016/j.physb.2018.04.009>
18. Sakhno O, Yezhov P, Hryn V, Rudenko V, Smirnova T (2020) Optical and nonlinear properties of photonic polymer nanocomposites and holographic gratings modified with noble metal nanoparticles. *Polymers (Basel)* 12:480. <https://doi.org/10.3390/polym12020480>
19. Ghosh D, Chattopadhyay N (2015) Gold and silver nanoparticles based superquenching of fluorescence: a review. *J Lumin* 160:223–232. <https://doi.org/10.1016/j.jlumin.2014.12.018>
20. Kazemifard S, Naji L, Taromi F (2018) Enhancing the photovoltaic performance of bulk heterojunction polymer solar cells by adding rhodamine b laser dye as co-sensitizer. *J Colloid Interface Sci* 515:139–151. <https://doi.org/10.1016/j.jcis.2018.01.018>
21. Sarkar A, Venkataraj R, Nampoori V, Kailasnath M (2019) Silver nanoparticles filled hollow polymer fiber laser with enhanced photostability. *Opt Laser Technol* 112:255–260. <https://doi.org/10.1016/j.optlastec.2018.11.016>
22. Koppal V, Patil P, Melavanki R, Kusanur R, Afi U, Patil N (2019) Exploring the influence of silver nanoparticles on the mechanism of fluorescence quenching of coumarin dye using fret. *J Mol Liq*. <https://doi.org/10.1016/j.molliq.2019.111419>
23. Krasovskii V, Karavanskii V (2008) Surface plasmon resonance of metal nanoparticles for interface characterization. *Opt Mem Neural Net* 17:8–14. <https://doi.org/10.1007/s12005-008-1002-x>
24. Krajczewski J, Kołataj K, Kudelski A (2017) Plasmonic nanoparticles in chemical analysis. *RSC Adv* 7:17559–17576. <https://doi.org/10.1039/c7ra01034f>
25. Rucha D, Mankad V, Gupta S, Jha P (2012) Size distribution of silver nanoparticles: uv-visible spectroscopic assessment. *Nanosci Nanotechnol Lett* 4:30–34. <https://doi.org/10.1166/nnl.2012.1278>
26. Bharathi D, Josebin M, Vasantharaj S, Bhuvaneshwari V (2018) Biosynthesis of silver nanoparticles using stem bark extracts of diospyros montana and their antioxidant and antibacterial activities. *J Nanostruct Chem* 8:83–92. <https://doi.org/10.1007/s40097-018-0256-7>
27. Mollick M, Bhowmick B, Maity D, Mondal D, Bain M, Bankura K, Sarkar J, Rana D, Acharya K, Chattopadhyay D (2012) Green synthesis of silver nanoparticles using paederia foetida l. leaf extract and assessment of their antimicrobial activities. *Int J Green Nanotechnol* 4:230–239. <https://doi.org/10.1080/19430892.2012.706103>
28. Tripathi J, Tripathi S, Keller J, Das K, Shripathi T (2013) Degradation study on structural and optical properties of annealed rhodamine b doped poly(vinyl) alcohol films. *Polym Degrad Stab* 98:12–21. <https://doi.org/10.1016/j.polymdegradstab.2012.11.003>
29. Karthik L, Kumar G, Kirthi A, Rahuman A, Rao K (2013) streptomyces sp. lk3 mediated synthesis of silver nanoparticles and its biomedical application. *Bioprocess Biosyst Eng* 37:261–267. <https://doi.org/10.1007/s00449-013-0994-3>
30. Jain S, Mehata M (2017) Medicinal plant leaf extract and pure flavonoid mediated green synthesis of silver nanoparticles and their enhanced antibacterial property. *Sci Rep* 7:1–13. <https://doi.org/10.1038/s41598-017-15724-8>
31. Paul B, Bhuyan B, Purkayastha D, Dhar S (2016) Photocatalytic and antibacterial activities of gold and silver nanoparticles synthesized using biomass of parkia roxburghii leaf. *J Photochem Photobiol, B* 154:1–7. <https://doi.org/10.1016/j.jphotochem.2015.11.004>
32. Deng H, Yu H (2018) self-assembly of rhodamine 6g on silver nanoparticles. *Chem Phys Lett* 692:75–80. <https://doi.org/10.1016/j.cplett.2017.12.003>

Publisher's Note Springer Nature remains neutral with regard to jurisdictional claims in published maps and institutional affiliations.